Cooperative dynamics of microtubule ensembles: Polymerization forces and rescue-induced oscillations

Björn Zelinski and Jan Kierfeld
Physics Department, TU Dortmund University, 44221 Dortmund, Germany
(Received 31 October 2011; revised manuscript received 5 November 2012; published 4 January 2013)

We investigate the cooperative dynamics of an ensemble of N microtubules growing against an elastic barrier. Microtubules undergo so-called catastrophes, which are abrupt stochastic transitions from a growing to a shrinking state, and rescues, which are transitions back to the growing state. Microtubules can exert pushing or polymerization forces on an obstacle, such as an elastic barrier, if the growing end is in contact with the obstacle. We use dynamical mean-field theory and stochastic simulations to analyze a model where each microtubule undergoes catastrophes and rescues and where microtubules interact by force sharing. For zero rescue rate, cooperative growth terminates in a collective catastrophe. The maximal polymerization force before catastrophes grows linearly with N for small N or a stiff elastic barrier, in agreement with available experimental results, whereas it crosses over to a logarithmic dependence for larger N or a soft elastic barrier. For a nonzero rescue rate and a soft elastic barrier, the dynamics becomes oscillatory with both collective catastrophe and rescue events, which are part of a robust limit cycle. Both the average and maximal polymerization forces then grow linearly with N, and we investigate their dependence on tubulin on-rates and rescue rates, which can be involved in cellular regulation mechanisms. We further investigate the robustness of the collective catastrophe and rescue oscillations with respect to different catastrophe models.

DOI: 10.1103/PhysRevE.87.012703 PACS number(s): 87.16.Ka

I. INTRODUCTION

Microtubules (MTs) are long and stiff filamentous proteins, which assemble and disassemble from tubulin dimers and serve various functions in the cytoskeleton: MT stiffness plays an important role in cytoskeletal mechanics but they also serve as "tracks" for intracellular transport by molecular motors. Finally, MTs exhibit an unusual polymerization dynamics, which is essential for spatial organization and remodelling processes in the cytoskeleton [1].

Polymerizing MTs can also generate pushing forces within the cell, because MTs grow by tubulin insertion also in the presence of an obstacle which exerts an opposing force on tubulin dimers inserted at the growing MT tip. The opposing force is transmitted onto the MT, as has been demonstrated in single-MT buckling experiments in front of a solid wall [2]. The force slows down further MT growth because monomer insertion against a force involves additional mechanical work. Growth finally terminates under a maximal polymerization force, which is typically in the pN range [2].

An important and unique feature of the MT polymerization dynamics is their so-called *dynamic instability*. The dynamic instability gives rise to phases of fast shrinking, which stochastically interrupt polymerization phases [3]. Each phase of of fast shrinking is initiated by a catastrophe event and terminated by a rescue event. This complex dynamic behavior is central to rapid remodelling in the cytoskeleton but also affects the polymerization force.

Catastrophe and rescue events of MTs are associated with guanosine triphosphate (GTP) hydrolysis within the MT [3]. Each tubulin dimer consists of an α- and β-tubulin and contains two GTP binding sites. Tubulin dimers assemble into polar MTs with a fast-growing plus end. GTP-tubulin dimers attach to the plus end with both binding sites containing GTP. The GTP in the α-tubulin is hydrolyzed to guanosine diphosphate (GDP) within the MT. This process leads to the formation of a GTP cap at the growing plus end, whereas the remaining MT consists of GDP-tubulin. The size of the GTP cap fluctuates in time and depends on the interplay of GTP-tubulin on-rate and hydrolysis rates within the MT. The GTP cap stabilizes the MT structure mechanically, and catastrophes are triggered by the loss of the GTP cap. The catastrophe rate therefore is related to the hydrolysis dynamics within the MT and given by the first passage rate to a state with vanishing GTP cap. There are different models describing this process [4–6], which will be discussed in Sec. II B in more detail. The dynamic instability also limits the ability of MTs to generate polymerization forces [7].

In a living cell, MTs often cooperate in order to generate higher forces. Cooperative MT polymerization forces play an important role during mitosis in generating forces necessary for chromosome separation [8]. A strong cooperativity in the dynamics of MTs is also relevant in processes regulating the cell length, as has been reported in Ref. [9] for animal cells. MTs also cooperate in the formation of cell protrusions, for example, in neuronal growth [10]. Therefore, it is important to develop models and a theoretical framework for the dynamics of MT ensembles under force, which can describe cooperative effects in the polymerization dynamics and quantify the cooperatively generated MT forces.

Only recently has it become possible to study force generation by MT ensembles *in vitro* using MT bundles growing against an elastic force, which was realized by an optical trap [11]. Experimental conditions were such that no rescue events occurred. The experiments showed *collective catastrophes* of the whole MT bundle: Before a collective catastrophe, a large fraction of the MT ensemble is growing cooperatively against the elastic force; growth often terminates in a catastrophe of the whole bundle where all pushing MTs nearly simultaneously undergo a catastrophe. In the experiments in Ref. [11], the maximal polymerization force

that is reached before a collective catastrophe was measured to grow linearly with the number N of MTs in the ensemble.

In Ref. [11], the experimentally observed collective catastrophes, and the linear N dependence, could be reproduced in simulations, where polymerizing MTs grow against an elastic force and interact by force sharing. A theory explaining the characteristic linear dependence of the maximal polymerization force on the number N of MTs is, however, lacking. The simulations in Ref. [11] included renucleation of MTs after complete depolymerization, which led to oscillations in the growth dynamics of the MT ensemble. The simulations did not include rescue events, which can be relevant *in vivo*.

In the present article, we will use a model for the collective dynamics of N MTs growing against an elastic barrier which is very similar to the model that has been used in the simulations in Ref. [11]. As in Ref. [11], the ensemble of MTs grow against an elastic force, which models the optical traps used in the experiments or the elastic cell cortex *in vivo*. As in Ref. [11], the most important features of the model are that MTs only interact by force sharing between the cooperatively pushing leading MTs and that the single-MT catastrophe rate increases exponentially with its load force. In contrast to Ref. [11], we will not consider renucleation of shrinking MTs but include rescue events into the model, which are an essential part of MT dynamics, and study their influence on the cooperative MT dynamics.

Furthermore, we also develop a dynamical mean-field theory, which provides a theoretical framework to describe the cooperative MT dynamics both in the absence and presence of rescue events. It allows us to extract the relevant control parameters, such as tubulin on-rate, rescue rate, and MT number, and to investigate their influence on dynamics and force generation. It is shown that, apart from collective catastrophes, also collective rescue events emerge if rescue events are taken into account in the single-MT dynamics. The resulting interplay between collective catastrophes and collective rescue events gives rise to an oscillatory growth dynamics of the entire MT ensemble. The dynamical mean-field theory successfully describes this oscillatory dynamics as a robust limit cycle.

The dynamical mean-field theory allows us to calculate the cooperative polymerization force generated by the MT ensemble and its dependence on the MT number N, the stiffness of the barrier, and the MT growth parameters. Furthermore, we use the dynamical mean-field theory to investigate the robustness of our results against variations of the catastrophe model. This is an important question as at least two different catastrophe models have been put forward in the literature and have been shown to describe experimentally available data on single-MT catastrophe rates. Robustness of our results show that details of the catastrophe models are not essential for force generation by ensembles of MTs but only rather general features, such as the exponential increase of the catastrophe rate with force, are relevant. We corroborate all our mean-field results by microscopic stochastic simulations of the full MT ensemble dynamics.

The paper is structured as follows. In Sec. II, we introduce the model describing the stochastic growth dynamics of an ensemble of N MTs growing against an elastic barrier. We, first, outline the stochastic growth model for a single MT, the catastrophe models used throughout the work, and, finally, the coupling between the N MTs in the ensemble dynamics via force sharing between leading MTs. In Sec. III we describe our choice of model parameters and describe the simulation.

We then develop the dynamical mean-field theory for this stochastic model. In Sec. IV, we start with the case of zero rescue rate, which has direct applications to the experiments by Laan *et al.* [11] and for which the cooperative MT dynamics is conceptually simpler to understand because there are only collective catastrophes. For zero rescue rate, we discuss the maximal polymerization force and find a linear N dependence for small N or stiff barriers with a crossover to a logarithmic dependence for large N or soft barriers. The results agree with the experimental findings of Ref. [11].

In Sec. V, we introduce the dynamical mean-field theory for the full problem in the presence of rescue events, where the cooperative MT dynamics exhibits both collective catastrophes and collective rescue events. For nonzero rescue rate and a soft barrier, we find stable collective catastrophe and rescue oscillations with maximal and average polymerization forces growing linearly with N. We show that our theory is applicable to different catastrophe models for single MTs and that our main findings are robust for catastrophe models with catastrophe rates exponentially increasing with force.

Throughout the article, we show that all theoretical results are in agreement with microscopic stochastic simulations.

II. MODEL FOR COOPERATIVE DYNAMICS OF MT ENSEMBLES

A. Single-MT model

The dynamic instability causes the MT plus end to switch stochastically between a growing (+) and a shrinking (–) state [12]. In the growing state, GTP-tubulin dimers (called *monomers* in the following) attach and detach with rates ω_{on} and ω_{off}, respectively, to one of the 13 protofilaments. The MT growth velocity in the growing state and in the absence of external forces is $v_+ = d(\omega_{\text{on}} - \omega_{\text{off}})$ [$v_+ = 1 \ldots 5 \times 10^{-8}$ m/s], where $d \simeq 8$ nm/13 is the effective monomer size.

Under force, the MT growth velocity becomes force dependent,

$$v_+(F) = d[\omega_{\text{on}} e^{-F/F_0} - \omega_{\text{off}}], \tag{1}$$

with a characteristic force, $F_0 \equiv k_B T/d \simeq 7$ pN. For simplicity, we assume that force only affects the on-rate of tubulin monomers. Experimental measurements of the force-velocity relation in Ref. [2] gave a significantly smaller value, $F_0 \simeq 2$ pN.

B. Dynamic instability and catastrophe models

The dynamic instability of MTs is associated with the loss of the stabilizing GTP cap because of hydrolysis within the MT [3]. At the catastrophe rate ω_c the MT loses its GTP cap in the growing state and switches into a state of fast shrinking with a large shrinking velocity v_- ($\simeq 3 \times 10^{-7}$ m/s). With the rescue rate ω_r the MT switches back from the shrinking into the growing state.

The catastrophe rate is related to the hydrolysis dynamics within the MT and given by the first passage rate to a state

with vanishing GTP cap. The resulting catastrophe rate has been discussed based on a model for *cooperative* hydrolysis of GTP-tubulin by Flyvbjerg *et al.* [4,5]. Similar cooperative models have been proposed for the hydrolysis dynamics in filamentous actin [13,14]. In a cooperative model, hydrolysis proceeds by a combination of both *random* and *vectorial* mechanisms. In a random mechanism, the hydrolysis rate r per length ($\simeq 3.7 \times 10^6\,\mathrm{m^{-1}\,s^{-1}}$) of GTP-tubulin is independent of the position of the GTP monomer in the MT. In a vectorial mechanism, only GTP monomers are hydrolyzed which have already hydrolyzed GDP monomers at one neighboring site. This results in a directed motion of GTP- and GDP-tubulin interfaces with mean velocity v_h ($\simeq 4.2 \times 10^{-9}$ m/s). The inverse catastrophe rate ω_c^{-1} can be obtained as mean first passage time to a state with a vanishing GTP cap. For a cooperative model, the exact analytical result for ω_c has been obtained in Refs. [4,5] as implicit function of the growth velocity v_+ and the hydrolysis parameters v_h and r. The exact dimensionless catastrophe rate $\alpha \equiv \omega_c D^{-1/3} r^{-2/3}$ is given by the smallest solution of

$$\mathrm{Ai}'(\gamma^2 - \alpha) = -\gamma\,\mathrm{Ai}(\gamma^2 - \alpha) \tag{2}$$

with $\gamma \equiv v D^{-2/3} r^{-1/3}/2$, where $v \equiv v_+ - v_h$ and $D \equiv (v_+ + v_h)d/2$ [$\mathrm{Ai}'(x) \equiv d\mathrm{Ai}(x)/dx$]. Here Ai denotes the first Airy function [15]. We use a numerical implementation of this exact analytical result for ω_c in simulations and mean-field calculations: We solve (2) to calculate the function $\alpha = \omega_c D^{-1/3} r^{-2/3}$ as a function of γ numerically. From this numerical solution we obtain the function $\omega_c = \omega_c(v_+)$, for which we generate an accurate interpolating polynomial of high order. This polynomial is used in the simulation to calculate catastrophe rates as a function of (force-dependent) growth velocity, $v_+(F)$. The remaining hydrolysis parameters v_h and r are fixed during the simulation.

The catastrophe rate ω_c becomes force dependent via the force dependence (1) of the growth velocity. The resulting catastrophe rate is a nonlinear and monotonically increasing function of the force F (see Fig. 1), which increases exponentially above the characteristic force F_0. We use the theoretical value $F_0 = k_B T/d \simeq 7$ pN for the model by Flyvbjerg *et al.* in the following.

We will investigate whether collective catastrophe and rescue oscillations are robust with respect to the catastrophe model. Different catastrophe models have been proposed and have been shown to describe experimentally available data on single-MT catastrophe rates. One alternative phenomenological catastrophe model has been proposed by Janson *et al.* based on experimental data for the inverse catastrophe rate, i.e., the average catastrophe time $\tau_c = 1/\omega_c$ [6]. The experimental data show that τ_c increases linearly with the growth velocity v_+ such that the catastrophe rate is given by

$$\omega_c = \frac{1}{a + b v_+}, \tag{3}$$

with $a \simeq 20$ s and $b \simeq 1.4 \times 10^{10}\,\mathrm{s^2\,m^{-1}}$ [6].

Also within the catastrophe model by Janson *et al.*, the catastrophe rate ω_c becomes force dependent via the force dependence (1) of the growth velocity, and the resulting catastrophe rate is a nonlinear and increasing function of the force F (see Fig. 1), which increases exponentially above the characteristic force F_0.

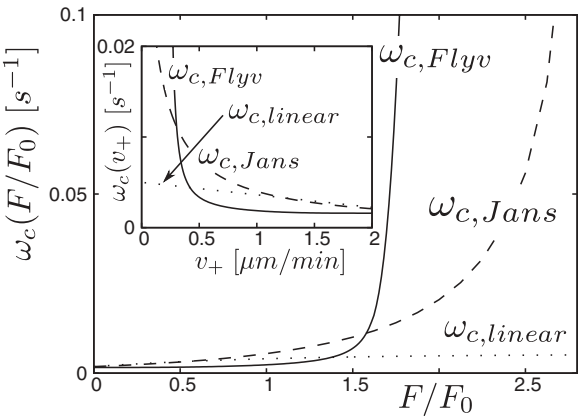

FIG. 1. The catastrophe rate ω_c (in $\mathrm{s^{-1}}$) as a function of the load force F (in units of F_0) for the Flyvbjerg model (with $F_0 \sim 7$ pN and for $\omega_{\mathrm{on}} = 70\ \mathrm{s^{-1}}$), the linear catastrophe model (with $\tilde{a} = 0.005\ \mathrm{s^{-1}}$, $\tilde{b} = 8 \times 10^5\ \mathrm{m^{-1}}$, $F_0 \sim 7$ pN, and $\omega_{\mathrm{on}} = 70\ \mathrm{s^{-1}}$), and the Janson model (with $F_0 \sim 0.8$ pN). Inset: The catastrophe rate ω_c (in $\mathrm{s^{-1}}$) as a function of the growth velocity v_+ (in μm/min) for the three different catastrophe models.

In the simulations of MT ensembles under force in Ref. [11], this catastrophe model is used in combination with a characteristic force $F_0 \simeq 0.8$ pN based on the experimental data in Ref. [2]; this value is significantly smaller than the theoretical value $F_0 = k_B T/d \simeq 7$ pN. For simulations, a 10-fold increased catastrophe rate is used in Ref. [11]. The other parameter values used in Ref. [11] are $v_{\mathrm{on}} = \omega_{\mathrm{on}}$, $d = 4.37 \times 10^{-8}$ m/s, which corresponds to $\omega_{\mathrm{on}} \approx 70\ \mathrm{s^{-1}}$ [2,11]. We will use the same set of parameters, apart from the 10-fold increase of the catastrophe rate, i.e., a small value $F_0 \simeq 0.8$ pN for our simulations with the catastrophe model by Janson *et al.*

Both the Flyvbjerg and Janson catastrophe models describe available experimental data on *single* MTs, as has been shown in Refs. [4,5] and [6], respectively. Therefore, it is important to investigate whether they also give compatible results for the *collective* dynamics of MTs under force.

In both models the catastrophe rate ω_c decreases as a power law over a wide range of growth velocities,

$$\omega_c \propto v_+^{-2/3}(\text{Flyvbjerg}), \quad \omega_c \propto v_+^{-1}(\text{Janson}). \tag{4}$$

Because of $v_+ \sim d\omega_{\mathrm{on}} e^{-F/F_0}$ for large velocities, ω_c increases exponentially with force F above the characteristic force F_0 in both catastrophe models. This can also be seen in the comparison in Fig. 1.

Our theory will predict collective catastrophe and rescue oscillations of the MT ensemble for all catastrophe models which fulfill two conditions:

(i) Force dependence via growth velocity: The catastrophe rate $\omega_c = \omega_c(v_+)$ is a function of the growth velocity and becomes force dependent via the force dependence of the growth velocity, $\omega_c = \omega_c(v_+(F))$; if single-MT catastrophes are related to hydrolysis within the MT and the loss of the stabilizing GTP cap, ω_c should be a *decreasing* function of v_+ and, thus, an *increasing* function of the force F.

(ii) Exponential force dependence above F_0: The resulting force dependence of ω_c is such that $Fd\omega_c/dF \gg \omega_c(F)$ for $F > F_0$ above the characteristic force F_0 [see also Eq. (24)]. This gives rise to a catastrophe rate that increases exponentially with force above the characteristic force F_0.

Requirement (ii) is fulfilled for all catastrophe rates decreasing as a power law $\omega_c \propto v_+^{-\varepsilon}$ ($\varepsilon > 0$) with growth velocity as in both the Flyvbjerg and Janson models; see Eq. (4). Accordingly, we will find collective catastrophe and rescue oscillations for both models.

It is possible to consider other types of catastrophe models where the catastrophe rate $\omega_c = \omega_c(v_+)$ is a decreasing function of the growth velocity according to requirement (i) but where requirement (ii) of an exponentially increase of the catastrophe rate with force is violated. One particularly simple example is a catastrophe rate which decreases *linearly* with velocity,

$$\omega_c(v_+) = \tilde{a} - \tilde{b}v_+. \tag{5}$$

We will demonstrate that collective catastrophe and rescue oscillations are indeed absent for such a "linear model." We will not discuss more elaborate multistep catastrophe models with more than two MT states, which have been proposed only recently [16].

C. Model for MT ensemble

We consider an ensemble of N parallel MTs, directed along the x direction. The ensemble is growing in a positive x direction and pushing against an elastic barrier, as shown in Fig. 2. The cooperative dynamics is governed by the number $n_+ < N$ of leading MTs which push simultaneously in the growing state.

The elastic barrier is modelled as a spring with equilibrium position $x_0 = 1\,\mu$m and a spring constant k in the range 10^{-7} N/m (soft) to 10^{-5} N/m (stiff as in the optical trap experiments in Ref. [11]). Barrier displacement by the leading MTs with their tips positioned at $x > x_0$ causes a force $F = F(x) = k(x - x_0)$ resisting further growth; for $x < x_0$ there is a force-free region. We assume that the force F is equally shared between all n_+ leading MTs such that each leading MT is subject to a force F/n_+. Force sharing is the only coupling between the MTs. In the presence of rescue events, i.e., for nonzero rescue rate, we force MTs shrinking to $x = 0$ to undergo rescue.

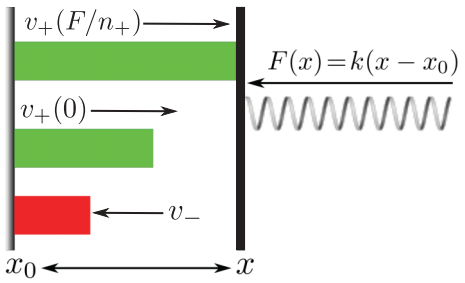

FIG. 2. (Color online) Schematic representation of $N = 3$ MTs for $n_+ = 1$. From top to bottom: MTs under force $F = k(x - x_0)$ grow with velocity $v_+(F/n_+)$ and unloaded MTs with $v_+(0)$. MTs shrink with v_- after a catastrophe.

Under a shared force F/n_+, the growth velocity of a MT reduces to $v_+(F/n_+) = d[\omega_{\rm on}e^{-F/n_+F_0} - \omega_{\rm off}]$ with the characteristic force $F_0 = k_BT/d$ governing monomer attachment; see Eq. (1). The force-dependent growth velocity also gives rise to a catastrophe rate $\omega_c = \omega_c(v_+(F/n_+))$ increasing with force. All nonleading MTs grow with the higher zero force velocity $v_+(0)$ in their growing state. Therefore, nonleading MTs, which grow force free and fast, "catch up" leading MTs, which grow under force with reduced velocity. This mechanism supports a state of collective growth, where a relatively large number n_+ of MTs are pushing cooperatively. We assume that the shrinking velocity v_- is independent of force. Because the catastrophe rate depends on force only via v_+, the relevant force scale of the problem is set by the characteristic force F_0; see (1).

This model for the dynamics of the MT ensemble is very similar to the model underlying the simulations in Ref. [11]. In particular, we use the same rules for the coupling between MTs by the load force. The most important difference is that we include rescue events in the single-MT dynamics, which have not been considered in Ref. [11].

III. MODEL PARAMETERS AND SIMULATION

In the simulation model the following parameters for MT growth have to be specified:

(i) The effective GTP-tubulin monomer size d, which is $d = 8$ nm/13 $= 0.6$ nm for 13 protofilaments.

(ii) The characteristic force F_0 governing the exponential decrease (1) of the single-MT growth velocity with force. We use $F_0 = k_BT/d \simeq 7$ pN in the Flyvbjerg catastrophe model and the measured value $F_0 \simeq 0.8$ pN [2] in the Janson catastrophe model.

(iii) We use a GTP-tubulin monomer off-rate of $\omega_{\rm off} = 6\ {\rm s}^{-1}$ [17]. Then the growth velocity in the absence of force $v_+(0) = d(\omega_{\rm on} - \omega_{\rm off})$ determines the GTP-tubulin monomer on-rate $\omega_{\rm on}$ (which is proportional to the GTP-tubulin concentration C_T).

(iv) Within the cooperative hydrolysis model by Flyvbjerg [4,5], the catastrophe rate ω_c is determined by the growth velocity v_+ [according to (1) with $F_0 = k_BT/d \simeq 7$ pN] and the hydrolysis parameters $v_h = 4.2 \times 10^{-9}$ m/s and $r = 3.7 \times 10^6\ {\rm m}^{-1}\,{\rm s}^{-1}$ [5]. The exact catastrophe rate is calculated from the numerical solution of Eq. (2) for given v_+, v_h, and r, as explained in Sec II B above.

(v) Within the hydrolysis model by Janson [6], the catastrophe rate ω_c is determined by the growth velocity v_+ [according to (1) with $F_0 \simeq 0.8$ pN] and the parameters $a \simeq 20$ s and $b \simeq 1.4 \times 10^{10}{\rm s}^2\,{\rm m}^{-1}$.

(vi) The shrinking velocity $v_- = 3 \times 10^{-7}$ m/s.

(vii) The rescue rate ω_r.

(viii) For the elastic force $F = k(x - x_0)$ on the leading MTs we use a spring stiffness $k = 10^{-7}$ N/m for a soft elastic barrier and $k = 10^{-5}$ N/m for a stiff elastic barrier as in the optical trap experiments in Ref. [11]. The rest position x_0 of the spring is taken as $x_0 = 1\ \mu$m. For nonzero rescue rate, we also use reflecting boundary conditions at $x = 0$, i.e., a filament undergoes immediate rescue if it shrinks to $x = 0$.

The parameters v_-, $\omega_{\rm off}$, v_h, and r are fixed in simulations. We vary the on-rate $\omega_{\rm on}$ and, thus, $v_+(0)$ and the rescue rate

TABLE I. Literature values for MT growth parameters $v_+(0)$, $\omega_{\rm on}$, v_-, and ω_r. TUB: *in vitro* results for tubulin solutions; Cell: *in vivo* results; microtubule associated proteins (MAPS): effect from MT associated proteins. Values for $\omega_{\rm on}$ are estimated from measured growth velocities via $\omega_{\rm on} \approx v_+(0)N/d$ neglecting $\omega_{\rm off}$.

Ref.	$v_+(0)$ (m/s)	$\omega_{\rm on}$ (1/s)	v_- (m/s)	ω_r (1/s)
Drechsel [18]	$(0.7 \ldots 2) \times 10^{-8}$	$(11 \ldots 32)$	$\sim 1.8 \times 10^{-7}$	—
Gildersleeve [19]	$\sim 4.2 \times 10^{-8}$	~ 68	$\sim 4.2 \times 10^{-7}$	—
Walker [20]	$(4 \ldots 8) \times 10^{-8}$	$(63 \ldots 130)$	$\sim 5 \times 10^{-7}$	$(0.05 \ldots 0.08)$(TUB)
Laan [11]	$\sim 4.2 \times 10^{-8}$	68.25	—	—
Janson [17]	$(3 \ldots 4.3) \times 10^{-8}$	$(53 \ldots 74)$	—	—
Pryer [21]	—	—	—	$\ldots 0.5$ (TUB) $\ldots 0.15$ (MAPS)
Dhamodharan [22]	—	—	—	$\ldots 0.07$ (Cell) $\ldots 0.085$ (MAPS)
Nakao [23]	—	—	—	$\ldots 0.1$ (TUB)
Shelden [24]	—	—	—	$(0.03 \ldots 0.2)$ (Cell)

ω_r within parameter ranges, which are selected according to literature values collected in Table I.

In the simulation, we integrate the deterministic equation of motion for an ensemble of N MTs with continuous lengths x_i $(i = 1, \ldots, N)$ and include stochastic switching between growth and shrinking for each MT. In the integration we use a fixed time step $\Delta t = 0.1$ s, which is small enough to ensure $\omega_{c,r}\Delta t \ll 1$. In each time step, we have to determine the number n_+ of leading force-sharing MTs. This is done by regarding all growing MTs within a distance $v_+(F/n_+)\Delta t$ of the leading MTs as leading for the next time step. We can perform two kinds of averages: Averages $\langle \ldots \rangle$ are taken over many realizations, and averages $\overline{\ldots}$ are time averages.

IV. COLLECTIVE CATASTROPHES AT ZERO RESCUE RATE

We start the analysis with the case of zero rescue rate because this case is conceptually simpler to understand as rescue events are absent, and there are only collective catastrophes to be discussed. Furthermore, this case is particularly important because experimental data are available: In recent experiments, Laan *et al.* [11] showed that MT ensembles exhibit phases of collective growth followed by collective catastrophes, where all leading MT nearly simultaneously undergo a catastrophe. The experiments were performed on short time scales such that no rescue events occur. It was also observed that the maximal polymerization force before catastrophes grows linearly in N. We quantify these features based on a dynamical mean-field theory.

In an ensemble of N MTs the dynamic instability of individual MTs leads to stochastic fluctuations in the number n_+ of leading MTs. The force F changes by filament growth according to $\dot{F} = k\dot{x}$ with $\dot{x} = v_+(F/n_+)$ if the ensemble grows $(n_+ \geqslant 1)$ and $\dot{x} = -v_-$ if all MTs shrink $(n_+ = 0)$. In a state of collective growth, a stable mean number of MTs are pushing cooperatively, while the force F is increasing by growth against the elastic barrier. If the number n_+ of pushing MTs is reduced by an individual catastrophe, the force on the remaining $n_+ - 1$ leading MTs increases and, thus, their catastrophe rate $\omega_c(F/n_+)$ increases. A cascade of individual catastrophes—a *collective catastrophe*—can be initiated until a state $n_+ = 0$ is reached with all MTs shrinking. This is the final absorbing state of the system in the absence of rescue events.

The stochastic dynamics of n_+ in a growing phase in the absence of rescue events is described by a one-step master equation with backward rates $r_{n_+} = n_+\omega_c(F/n_+)$ for decreasing n_+ by one, which derive from the catastrophe rate of individual MTs under force sharing. In a mean-field approach, we replace the stochastic variables F and n_+ by their (time-dependent) mean values $\langle F\rangle$ and $\langle n_+\rangle$ (averaging over many realizations of the stochastic n_+ dynamics) and neglect all higher-order correlations, e.g., set $\langle F/n_+\rangle = \langle F\rangle/\langle n_+\rangle$. In the growing phase, we then obtain two coupled mean-field equations,

$$d\langle n_+\rangle/dt = -\langle n_+\rangle\omega_c(\langle F\rangle/\langle n_+\rangle), \tag{6}$$

$$d\langle F\rangle/dt = kv_+(\langle F\rangle/\langle n_+\rangle). \tag{7}$$

In the mean-field approximation we can calculate the maximal polymerization force $F_{\rm max}$ (averaged over many realizations) that is reached during the mean first passage time from $n_+ = N$ to $n_+ = 0$ by solving

$$\frac{d\langle F\rangle}{d\langle n_+\rangle} = \frac{d\langle F\rangle/dt}{d\langle n_+\rangle/dt} = -\frac{kv_+(\langle F\rangle/\langle n_+\rangle)}{\langle n_+\rangle\omega_c(\langle F\rangle/\langle n_+\rangle)}, \tag{8}$$

with initial conditions $\langle F\rangle = 0$ for $\langle n_+\rangle = N$ in order to find $\langle F\rangle = F_{\rm max}$ at $\langle n_+\rangle \approx 0$.

Above the characteristic force F_0, the ratio $v_+(F)/\omega_c(F)$ decays exponentially because $v_+(F)$ decreases exponentially and $\omega_c(v_+(F))$ increases exponentially. Therefore, we can solve in two steps: (i) As long as the shared force is small compared to F_0, $\langle F\rangle/\langle n_+\rangle \ll F_0$, we neglect the force and find $\langle F\rangle \approx kv_+(0)/\omega_c(0)\ln(N/\langle n_+\rangle)$. (ii) For $\langle F\rangle/\langle n_+\rangle \gg F_0$, on the other hand, the catastrophe frequency increases exponentially, and we can assume that $d\langle F\rangle/d\langle n_+\rangle \approx 0$ and $\langle F\rangle$ remains constant.

The boundary between regimes (i) and (ii) is determined by the condition $\langle F\rangle/\langle n_+\rangle = F_0$: Regime (i) applies for $\langle n_+\rangle > n_0$ with $n_0 = \alpha W(N/\alpha)$, where $W(x)$ is the Lambert W function, which is the solution of $x = We^W$ (for $W \geqslant -1$). The parameter

$$\alpha \equiv kv_+(0)/\omega_c(0)F_0 \tag{9}$$

is a dimensionless measure for the stiffness of the elastic barrier. Because $\langle F\rangle$ remains constant for $\langle n_+\rangle < n_0$, the

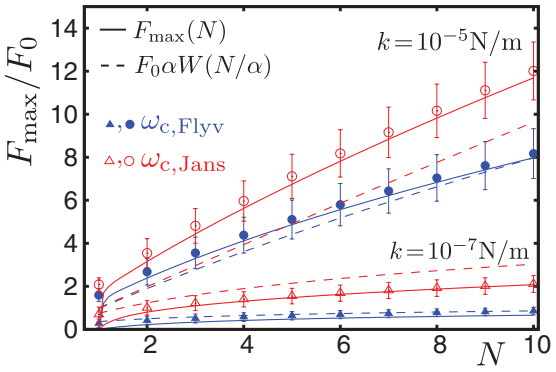

FIG. 3. (Color online) $F_{\max}/F_0$ as a function of N for zero rescue rate, $\omega_{\mathrm{on}} = 70\ \mathrm{s}^{-1}$, and $k = 10^{-7}$ N/m ($\alpha \simeq 2.7$, soft barrier) and $k = 10^{-7}$ N/m ($\alpha \simeq 27$, stiff barrier). We compare results for the catastrophe models of Flyvbjerg (blue, solid symbols) and Janson (red, open symbols). Data points are simulation results; error bars represent the standard deviation of the stochastic quantity $F_{\max}/F_0$. Solid lines are numerical solution of the mean-field dynamics (6) and (7). Dashed lines are analytical estimates according to (10).

resulting maximal polymerization force is given by

$$F_{\max} = n_0 F_0 = F_0 \alpha W(N/\alpha), \tag{10}$$

with a logarithmic asymptotics $F_{\max} \approx F_0 \alpha \ln(N/\alpha)$ for large $N \gg \alpha$ or a soft barrier and a quasilinear behavior $F_{\max} \approx F_0 N(1 - N/\alpha)$, which is *independent* of α to leading order, for small $N \ll \alpha$ or a stiff barrier. The mean-field result (10) agrees with numerical solutions of the mean-field dynamics as given by Eqs. (6) and (7) and full stochastic simulations both for soft and stiff barriers, as can be seen in Fig. 3.

The parameter α can also be interpreted as a measure for the relative speed of the initial $\langle n_+ \rangle$ and $\langle F \rangle$ dynamics according to the mean-field equations (6) and (7), which allows us to give simple arguments for the maximal polymerization force $F_{\max}$: For $\alpha \ll N$ (the case of a soft barrier), the $\langle n_+ \rangle$ dynamics is fast compared to the $\langle F \rangle$ dynamics. Therefore, $\langle n_+ \rangle$ decays approximately force free in a time $t_c \sim 1/\omega_c(0) \ln N$ from $\langle n_+ \rangle = N$ to $\langle n_+ \rangle = 1$. During this time, the force reaches a value $F_{\max} \sim k v_+(0) t_c \sim F_0 \alpha \ln N$. For $\alpha \gg N$ (the case of a stiff barrier), the $\langle n_+ \rangle$ dynamics is initially slow compared to the $\langle F \rangle$ dynamics and $\langle n_+ \rangle \approx N$ until the characteristic force F_0 per MT is reached and the catastrophe rate increases exponentially. Up to this point, essentially N MTs share the force such that F increases up to $F_{\max} \sim F_0 N$ until catastrophes set in. This takes a time $t_c \sim N F_0 / k v_+(0)$ and $\Delta \langle n_+ \rangle \sim \langle \dot{n_+} \rangle t_c \sim N/\alpha \ll 1$ is indeed small such that the assumption $\langle n_+ \rangle \approx N$ is consistent.

In the experiments in Ref. [11], the spring stiffness was $k \simeq 10^{-5}$ N/m, which gives $\alpha \simeq 27$ such that these experiments were performed in the quasilinear regime of a stiff barrier, where we predict $F_{\max} \approx F_0 N$ for all experimentally accessible N (see the upper lines in Fig. 3). This linear increase is in agreement with the experimental results but the ratio $F_{\max}/N$ is only of the order of 3 pN experimentally, while $F_0 \simeq 7$ pN. This hints at a lower value for F_0 in the force-polymerization velocity relation for MTs; experimentally, a value $F_0 \simeq 2$ pN has been measured in Ref. [2], which is indeed compatible with the experimental results of Ref. [11].

In Fig. 3, we compare mean-field theory and simulation results for the Flyvbjerg and the Janson catastrophe model for both soft and stiff barriers. For both models, we find agreement between mean-field theory and simulations and, moreover, both models give comparable values for generated forces. This demonstrates that results for the cooperative force generation at zero rescue rate are robust with respect to details of the single-MT catastrophe model. The essential feature entering the mean-field theory is the exponential increase of the catastrophe frequency with force above the characteristic force F_0.

V. COLLECTIVE CATASTROPHES AND COLLECTIVE RESCUE FOR NONZERO RESCUE RATE

We now consider force generation in the presence of rescue events. Rescue events were not included in the simulation model in Ref. [11]. Also experiments in Ref. [11] were performed on short time scales such that no rescue events occurred. However, rescue events are an essential part of MT dynamics, and their influence on force generation and MT dynamics needs to be addressed.

In the presence of rescue events, the dynamics will not change considerably for $N \ll \alpha$, i.e., for a stiff barrier because this limit corresponds to a *slow* $\langle n_+ \rangle$ dynamics, which cannot benefit from additional rescue events. Moreover, because the $\langle F \rangle$ dynamics is fast, rescue will not happen before the force-free region $x < x_0$ is reached, where MTs decouple.

Therefore, we focus on the influence of rescue events for $N \gg \alpha$ or a soft barrier corresponding to a *fast* $\langle n_+ \rangle$ dynamics. In this regime, the collective dynamics becomes strongly modified. Apart from collective catastrophes also collective rescue events occur: After a collective catastrophe the system is in a state $n_+ = 0$ with all MTs shrinking. Individual rescue events lead to $n_+ = 1$, but a single MT bearing the whole force undergoes an immediate catastrophe again with high probability. Therefore, a cascade of rescue events—a *collective rescue*—is necessary to increase n_+ back to a number sufficient to maintain stable collective growth.

A. Simulation results

Alternating collective catastrophes and collective rescue events give rise to oscillations in the polymerization force or, equivalently, the position x of the obstacle. Such oscillations with alternating collective catastrophes and collective rescue events can be clearly seen in the stochastic simulation trajectories for the positions x of the MTs [see Figs. 4(a) and 4(c)] and the number n_+ of leading MTs [see Figs. 4(b) and 4(d)] as a function of time t. The simulation trajectories also show that this phenomenon is robust with respect to the catastrophe model and can be observed both for the Flyvbjerg and the Janson catastrophe models, which are shown in Fig. 4 on the left and the right sides, respectively, and exhibit qualitatively very similar behavior. Similar oscillations have been observed in the simulations in Ref. [11] in the presence of MT renucleation instead of MT rescue and for a constant force.

In the simulations we measure the polymerization force $F_{\mathrm{s,N}} = \overline{\langle F \rangle}$, which is averaged over time and many realizations

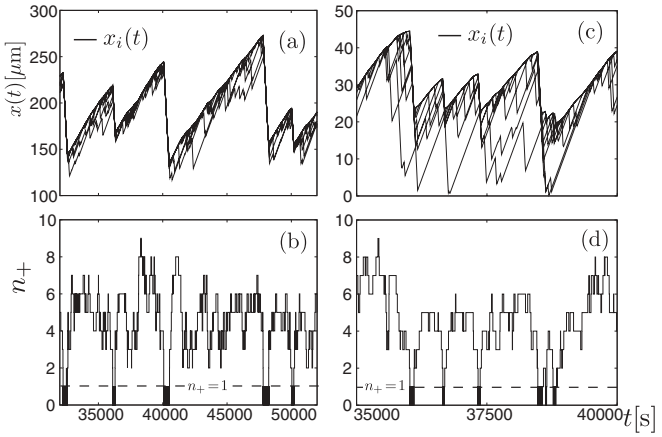

FIG. 4. Typical simulation trajectories for $N = 10$ MTs, $\omega_{on} = 70\ s^{-1}$, and $\omega_r = 0.05\ s^{-1}$; left [(a) and (b)] for the Flyvbjerg catastrophe model and right [(c) and (d)] for the Janson catastrophe model. [(a) and (c)] Positions of all MTs as a function of time t; the obstacle position $x(t)$ is the position of the leading MT. [(b) and (d)] The number n_+ of leading MTs as a function of time t. Collective catastrophes and collective rescue events can be clearly recognized: In a collective catastrophe n_+ drops to $n_+ = 1$ and $x(t)$ of the leading MTs starts to shrink; after a collective rescue n_+ starts to increase again to values $n_+ > 1$, and $x(t)$ of the leading MTs start to grow.

as a function of MT number N and of the on-rate ω_{on}. This time-averaged polymerization force is also the stall force of the MT ensemble. The results are shown in Fig. 5 for both the Flyvbjerg catastrophe model [upper row: Figs. 5(a) and 5(b)] and the Janson catastrophe model [lower row: Figs. 5(d) and 5(e)]. The main finding of the simulations is an approximately *linear* increase of the polymerization force $F_{s,N}$ with the number N of MTs [see Figs. 5(a) and 5(d)]. This shows that for large MT ensembles, rescue events give rise to much higher polymerization forces as compared to the logarithmic N dependence derived in the previous section in the absence of rescue events for a soft barrier ($N \gg \alpha$). Simulations also show an approximately linear increase of the polymerization force with the on-rate ω_{on} [see Figs. 5(b) and 5(e)].

We also show numerical results for the time-averaged pushing fraction $\overline{\nu_+} = \overline{\langle n_+ \rangle}/N$ of MTs as a function of the on-rate ω_{on} in Figs. 5(c) and 5(f). The pushing fraction increases with on-rate, which demonstrates an increasing tendency of MTs to push *synchronously* at higher on-rates, where larger forces are generated.

Simulation results for the Flyvbjerg model (upper row in Fig. 5) and the Janson model (lower row in Fig. 5) show a very similar linear increase for the polymerization force $F_{s,N}$ with N and very similar results for the time-averaged pushing fraction $\overline{\nu_+}$ of MTs, which is in accordance with the

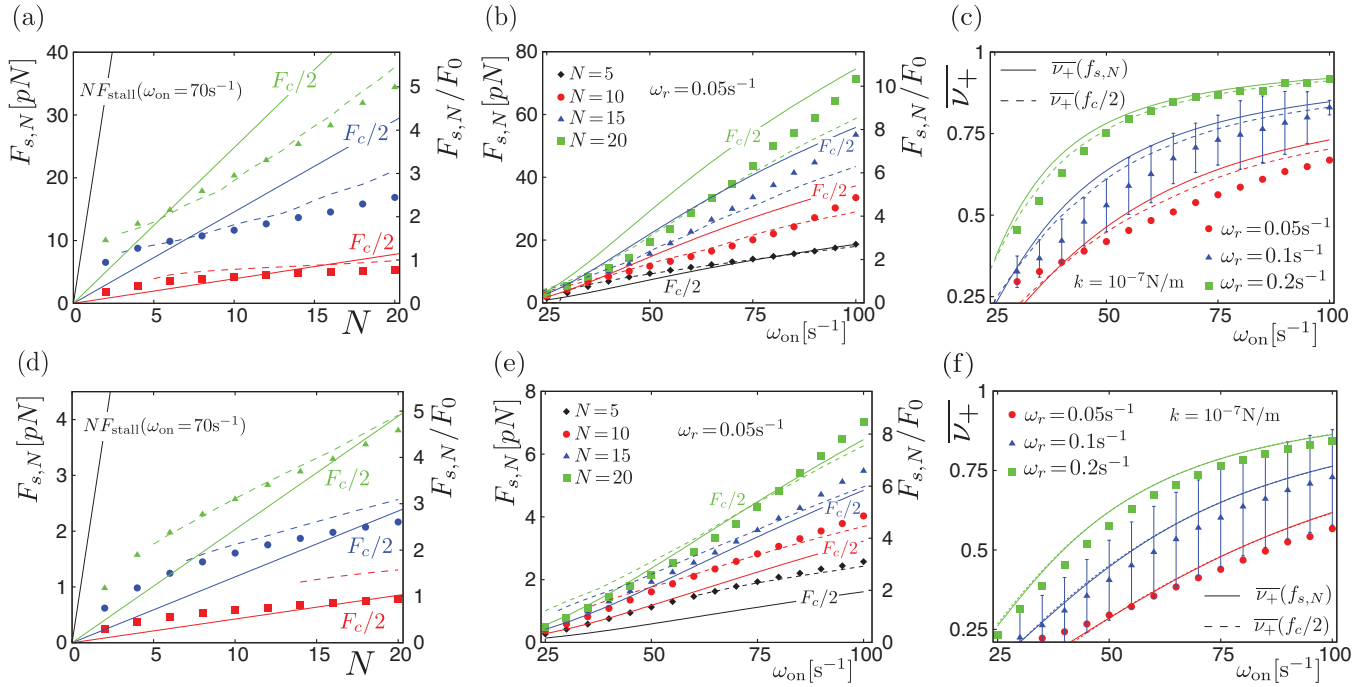

FIG. 5. (Color online) Upper row: Simulation results using the Flyvbjerg catastrophe model. Lower row: Simulation results using the Janson catastrophe model. Both are for a soft barrier ($k = 10^{-7}$ N/m). [(a) and (d)] Simulation results for the average polymerization force $F_{s,N}$ as a function of the number N of MTs for different on-rates $\omega_{on} = 30\ s^{-1}$(■), $50\ s^{-1}$(●), and $70\ s^{-1}$(▲) at a fixed rescue rate $\omega_r = 0.05\ s^{-1}$. Solid lines: Mean-field estimate $F_{s,N} = F_c/2$, see Eq. (23) (neglecting F_{min}). Dashed lines: Numerical mean-field solution including stochastic effects. Black solid line: N-fold single-MT stall force $F_{s,N} = NF_{stall}$ for $\omega_{on} = 70\ s^{-1}$. [(b) and (e)] Polymerization force $F_{s,N}$ as a function of on-rate ω_{on} for $N = 5$(♦),10(●),15(▲),20(■), and $\omega_r = 0.05\ s^{-1}$. Solid lines: Mean-field estimate $F_{s,N} = F_c(\omega_{on})/2$. Dashed lines: Numerical mean-field solution including stochastic effects. [(c) and (f)] Time-averaged pushing fraction $\overline{\nu_+} = \overline{\langle n_+ \rangle}/N$ of MTs as a function of ω_{on} for $\omega_r = 0.05\ s^{-1}$(●), $0.1\ s^{-1}$(▲), and $0.2\ s^{-1}$(■). Solid lines: Solution of Eq. (18) for $f = f_c/2$. Dashed lines: Solution of Eq. (18) for $f = F_{s,N}/N$ with $F_{s,N}$ from the numerical mean-field solution including stochastic effects. Error bars represent the standard deviation of the stochastic quantity $\overline{n_+}/N$. For reasons of clarity we only show error bars for $\omega_r = 0.1 s^{-1}$. All other standard deviations are of the same magnitude.

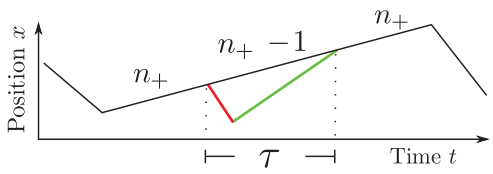

FIG. 6. (Color online) Illustration of time scale τ from Eq. (11).

qualitatively similar simulation trajectories shown in Fig. 4 for both catastrophe models. This further supports that our results are robust with respect to the catastrophe model. The absolute values of typical forces in Figs. 5(a), 5(b), 5(d), and 5(e) and, similarly, between typical MT lengths in Figs. 4(a) and 4(c) differ, however, between the two catastrophe models. The reason is that the basic force scale of the problem is the characteristic force F_0, above which the catastrophe rate increases exponentially, as will be shown below. We have chosen the theoretical value $F_0 = k_B T/d \simeq 7$ pN for the Flyvbjerg model and the much smaller value $F_0 = 0.8$ pN according to Ref. [11] with the Janson model. In units of the characteristic force F_0, typical forces are very similar [see Figs. 5(a), 5(b), 5(d), and 5(e) right scale].

B. Dynamical mean-field theory

We will show that all simulation results and the robustness with respect to the catastrophe model can be explained based on a dynamical mean-field theory.

In the presence of rescue events, the mean-field equation (6) for $\langle n_+\rangle$ becomes modified in the growing phase. The one-step master equation for n_+ in a growing phase also contains a forward rate $g_{n_+} = (N - n_+)\tau^{-1}$ for increasing n_+ by one. This forward rate is determined by a rescue and "catch-up" process for the $(N - n_+)$ MTs, which are not pushing: The time τ denotes the mean time that it takes for a MT to rejoin the group of n_+ pushing MTs after undergoing an individual catastrophe followed by rescue and force-free growth at a velocity $v_+(0)$ that is larger than the velocity $v_+(F/n_+)$ of the leading MTs under force (see Fig. 6). After a rescue time $1/\omega_r$ the trailing MT has to "catch up" a distance $[v_+(F/n_+) + v_-]/\omega_r$ to the leading MTs, which kept growing with velocity $v_+(F/n_+)$. Given a velocity difference $v_+(0) - v_+(F/n_+)$ to the leading MTs under force, this requires a time

$$\tau \approx \omega_r^{-1}[1 + (v_+(F/n_+) + v_-)/(v_+(0) - v_+(F/n_+))], \quad (11)$$

which is larger than the bare rescue time $1/\omega_r$. This results in a modified mean-field equation for $\langle n_+\rangle$,

$$d\langle n_+\rangle/dt = -\omega_c(\langle F\rangle/\langle n_+\rangle)\langle n_+\rangle + \langle\tau\rangle^{-1}(N - \langle n_+\rangle k), \quad (12)$$

where we have to apply the mean-field averaging also to $\langle\tau\rangle$ in Eq. (11),

$$\langle\tau\rangle \approx \omega_r^{-1}\left[1 + \frac{v_+(\langle F\rangle/\langle n_+\rangle) + v_-}{v_+(0) - v_+(\langle F\rangle/\langle n_+\rangle)}\right]. \quad (13)$$

Typically $\langle\tau\rangle$ is by a factor of 10 larger than the bare rescue time $1/\omega_r$.

C. Limit cycle oscillations and absence of bifurcations

For the further analysis of the mean-field dynamics it is advantageous to introduce new variables, the average force per MT f and the average fraction ν_+ of pushing MTs,

$$f \equiv \langle F\rangle/N, \quad \nu_+ \equiv \langle n_+\rangle/N \quad (14)$$

with $\langle F\rangle/\langle n_+\rangle = f/\nu_+$. Using these variables, the mean-field equations become

$$d\nu_+/dt = -\nu_+\omega_c(f/\nu_+) + (1 - \nu_+)/\langle\tau\rangle, \quad (15)$$

$$df/dt = k\nu_+(f/\nu_+)/N. \quad (16)$$

We first discuss the nullclines of f and ν_+, i.e., the contours in the f-ν_+ plane along which $df/dt = 0$ and $d\nu_+/dt = 0$ is satisfied, respectively.

The nullclines of f require $\nu_+(f/\nu_+) = 0$, which leads to a straight line,

$$f = \nu_+ F_{\text{stall}} \quad (17)$$

in the f-ν_+ plane, where the slope is given by the single-MT stall force $F_{\text{stall}} = F_0 \ln(\omega_{\text{on}}/\omega_{\text{off}})$ [see Fig. 7(a)].

The nullclines of ν_+ are given by

$$0 = g(f,\nu_+) \equiv -\nu_+\omega_c(f/\nu_+) + \frac{1}{\langle\tau\rangle(f/\nu_+)}(1 - \nu_+) \quad (18)$$

and are *independent* of N. The shape of the nullclines depends on the functional dependence of the catastrophe rate on the force and, thus, on the catastrophe model. We will first focus on the Flyvbjerg catastrophe model, for which the nullclines of ν_+ have a characteristic loop shape, as shown in Fig. 7, which exhibits two solution branches: a *stable* upper branch $\nu_{+,u}$ corresponding to a collectively growing state with $\langle n_+\rangle = N\nu_{+,u}$ pushing MTs and an *unstable* lower branch $\nu_{+,u}$. For a soft barrier, the $\langle n_+\rangle$ dynamics is fast, and the force increases slowly during collective growth, while $\nu_+ = \nu_{+,u}$ is tracing the stable upper branch of the nullcline. The force per MT can increase up to a critical value f_c (with a corresponding value ν_c for ν_+), where stable and unstable branch join and where the nullcline has vertical slope $df/d\nu_+ = 0$ in the f-ν_+ plane. The critical force $F_c = f_c N$ represents the maximal load force for which the MT ensemble can maintain a stable state of collective growth: for $\langle F\rangle > F_c$ the number $\langle n_+\rangle$ of pushing MTs has to flow spontaneously to a state $\langle n_+\rangle = 0$.

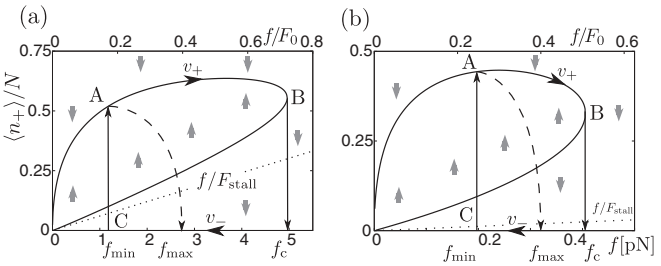

FIG. 7. Nullclines of the mean-field equations for (a) the Flyvbjerg model and (b) the Janson model for $\omega_{\text{on}} = 70\,\text{s}^{-1}$, $\omega_r = 0.05\text{s}^{-1}$, and $k = 10^{-7}$ N/m (soft barrier). The nullclines of $\nu_+ \equiv \langle n_+\rangle/N$ are solutions of Eq. (18) and assume a loop shape as a function of $f \equiv \langle F\rangle/N$. Gray arrows indicate the mean-field flow of $\langle n_+\rangle$. The nullcline for f is a straight line $\nu_+ = f/F_{\text{stall}}$. The critical force is $f_c = F_c/N \simeq 3$ pN for the Flyvbjerg model (a) and $f_c \simeq 0.4$ pN for the Janson model (b). Black arrows indicate the stable mean-field limit cycle (see text); dashed line indicates effect of stochastic fluctuations.

The critical force f_c per MT can be obtained from two conditions: (i) the nullcline equation $g(f,v_+)=0$, i.e., Eq. (18), and (ii) taking a total derivative with respect to v_+ and using the condition of a vertical slope $df/dv_+=0$, we arrive at the second condition, $\frac{\partial}{\partial v_+}g(f,v_+)=0$. Because $\omega_c(F)$ increases exponentially above F_0, see Eq. (4), $d\omega_c/dF \sim \omega_c/F_0$ is a good approximation. The effective rescue time $\langle\tau\rangle=\langle\tau\rangle(f/v_+)$ has a much weaker force dependence, which we neglect. These approximations give

$$\begin{aligned} 0 &\approx -\omega_c(f/v_+)\left(1-\frac{f}{v_+F_0}\right)-\frac{1}{\langle\tau\rangle(f/v_+)} \\ \frac{f}{v_+F_0} &\approx 1+\frac{1}{\omega_c(f/v_+)\langle\tau\rangle(f/v_+)}. \end{aligned} \tag{19}$$

It turns out that (for both the Flyvbjerg and the Janson catastrophe models) $\omega_c\langle\tau\rangle \geqslant 1$ holds over the entire range of forces. In order to estimate f_c, we assume $\omega_c\langle\tau\rangle \gg 1$. This leads to an estimate $\frac{f}{v_+}\approx F_0$ in Eq. (19), which can be used in the arguments of ω_c and $\langle\tau\rangle$. Solving the Eqs. (18) and (19) for f_c and v_c we find analytical estimates,

$$f_c \approx F_0\frac{1}{\omega_c(F_0)\,\langle\tau\rangle(F_0)}, \tag{20}$$

$$v_c \approx \frac{1}{1+\omega_c(F_0)\,\langle\tau\rangle(F_0)}. \tag{21}$$

According to Eqs. (17) and (18), the nullclines for f and v_+ and, thus, the critical values f_c and v_c, are strictly *independent* of N. Therefore, the critical total force $F_c=Nf_c$ has to be strictly *linear* in the number of MTs. The critical force is the maximal polymerization force that can be generated during polymerization in the presence of rescue events. For a soft barrier ($N \gg \alpha$), rescues thus lead to a significant increase in the maximal polymerization force with a linear N dependence compared to the logarithmic dependence derived above in the absence of rescue. Moreover, the estimate (20) for f_c predicts an increase of the generated force with the on-rate $\omega_{\rm on}$ because this increases v_+ and, thus, reduces ω_c and an increase with the rescue rate ω_r because this decreases $\langle\tau\rangle$ [see Eq. (11)].

In order to analyze the system for fixed points, we compare the lower branch $v_{+,l}$ of the nullcline of v_+ with the nullcline (17) of f. The lower branch is governed by the exponential increase $\omega_c(F)\sim\omega_c(0)\exp(cF/F_0)$ with force (with $c=2/3$ in the Flyvbjerg and $c=1$ in the Janson catastrophe model), resulting in $\omega_c(0)\exp(cf/v_+F_0)\sim 1/\langle\tau\rangle v_+$ or $f/v_+\approx F_0\ln(1/\omega_c(0)\langle\tau\rangle v_+)/c$. This is always at *lower* forces than the nullcline [Eq. (17)] of f because $F_{\rm stall}=F_0\ln(\omega_{\rm on}/\omega_{\rm off})\gg F_0\ln(1/\omega_c(0)\langle\tau\rangle v_+)/c$. This inequality can be violated only at very high rescue rates ω_r giving rise to a small $\langle\tau\rangle$. We obtained that $\omega_r \gg 1/s$ is necessary to obtain a fixed point. Only if this fixed point exists *and* is stable can it undergo a Hopf bifurcation on lowering the rescue rate. We conclude that, for realistic parameter values $\omega_r\sim 0.05\ {\rm s}^{-1}$, we are always far from a Hopf bifurcation.

The system rather *oscillates* in a *stable limit cycle*: After rescue [A in Fig. 7(a)], the pushing force f increases with the MT growth velocity because of $\dot f = kv_+/N$, while $v_+=v_{+,u}$ is tracing the stable branch of the nullcline. At the critical force level f_c, a collective catastrophe occurs [B in Fig. 7(a)], where the ensemble is quickly driven to collective shrinking with $\langle n_+\rangle=0$ or 1 and $\dot f=-kv_-/N$.

During shrinking the force level is reduced until an individual rescue event can initiate collective rescue at a force $F_{\rm min}$ [C in Fig. 7(a)]. During rescue $\langle n_+\rangle$ increases quickly back to its stable fixed point value [A in Fig. 7(a)], closing the limit cycle.

The collective rescue force $F_{\rm min}$ can be calculated from the condition that the lower unstable branch of fixed points given by Eq. (18) intersects the line $\langle n_+\rangle=1$, leading to the condition

$$N=\omega_c(F_{\rm min})\langle\tau\rangle(F_{\rm min})+1. \tag{22}$$

Collective rescue typically happens at rather small force $F_{\rm min}\ll F_0$ such that we find an essentially linear N dependence $F_{\rm min}\sim N+O(1)$.

The collective mean-field dynamics thus oscillates between forces $F_{\rm min}$ and F_c. The resulting time-averaged polymerization force

$$F_{\rm s,N}=\overline{\langle F\rangle}\approx(F_{\rm min}+F_c)/2 \tag{23}$$

is also *linear* in N. This is in agreement with the simulation results [see Figs. 5(a) and 5(c)]. Because $F_c\gg F_{\rm min}$ the result $F_c\approx NF_0/(\omega_c(F_0)\langle\tau\rangle(F_0))$ from Eq. (20) determines the dependence of the polymerization force $F_{s,N}$ on the on-rate $\omega_{\rm on}$ and the rescue rate ω_r. The estimate for F_c predicts an increase of the generated force with the on-rate $\omega_{\rm on}$ because this increases v_+ and, thus, reduces ω_c. For the velocity dependence (4) and assuming $v_+\propto\omega_{\rm on}$ (for $\omega_{\rm on}\gg\omega_{\rm on}$), Eq. (20) gives $F_c\propto\omega_{\rm on}^{2/3}$ for the Flyvbjerg catastrophe model (and $F_c\propto\omega_{\rm on}$ for the Janson catastrophe model), which is in qualitative agreement with the simulation result of an approximately linear increase of the polymerization force with the on-rate $\omega_{\rm on}$ in Figs. 5(a) and 5(d). From the result (20), we also predict an increase of the polymerization force with the rescue rate ω_r because this decreases $\langle\tau\rangle$. The pronounced increase of $F_{s,N}$ with the on-rate $\omega_{\rm on}$ demonstrates that for an MT ensemble, the polymerization force can be sensitively regulated by changing the concentration of available monomers. We also find the collective stall force $F_{s,N}$ always remains much smaller than the N-fold single-MT stall force, $F_{s,N}\ll NF_{\rm stall}$ [see Figs. 5(a) and 5(c)] in contrast to force-sharing filaments without dynamic instability, where $F_{s,N}=NF_{\rm stall}$ holds exactly [25]. A further confirmation of the mean-field theory is provided by simulation results for the time-averaged pushing fraction $\overline{v_+}=\overline{\langle n_+\rangle}/N$ in Figs. 5(c) and 5(f). Mean-field results for v_+ evaluated using the nullcline equation (18) for $f=F_{s,N}/N$ show good agreement with the simulations results.

The oscillatory limit cycle dynamics, which gives rise to collective catastrophe and rescue oscillations, is robust against perturbations because the system is far from a bifurcation for realistic rescue rates. Only for very high rescue rates, $\omega_r\gg 1/s$, does a stable fixed point exist, which becomes unstable in a Hopf bifurcation on lowering the rescue rate.

Similar collective catastrophes and rescues are also observed in *in vitro* bulk polymerization experiments [26,27]. In these experiments *many* MTs synchronously polymerize in a solution with GTP-tubulin concentration $c_{\rm GTP}$. All MTs share the available concentration $c_{\rm GTP}$ and grow with a velocity

$v_+(c_{\mathrm{GTP}})$, which decreases if GTP-tubulin is consumed. Here, collective catastrophes and rescues are caused by sharing the concentration c_{GTP} of available GTP-tubulin, resulting in similar collective oscillations as force-sharing induces in the present system.

Finally, we want to note that the collective dynamics for $N \gg 1$ that we described here differ markedly from the dynamics of a *single* MT ($N = 1$) [7]. For a single-MT rescue does not happen at a particular force level F_{min} but after an average time $1/\omega_r$ set by the individual rescue rate. The resulting $N = 1$ mean-field equation for the average force $\langle F\rangle$ is $v_-/\omega_r = v_+(\langle F\rangle)/\omega_c(\langle F\rangle)$ [7] and equals shrinking and growing distance between individual rescue and catastrophe events.

D. Robustness with respect to catastrophe models

An essential requirement for the existence of an oscillatory limit cycle is the loop shape of the nullclines of $\langle n_+\rangle$ according to the stationary mean-field equation (18) (see Fig. 7). Results presented so far have been derived from the Flyvbjerg model. We obtain a very similar loop-shaped nullcline also with the catastrophe model by Janson *et al.* [see Eq. (3)]. The condition for a loop-shape nullcline is the existence of a critical force F_c, where the two solution branches of Eq. (18) merge in a point with a vertical tangent. From Eq. (18), we can derive the necessary condition

$$0 < \tau^{-1} < \omega_c(F) - F\frac{d}{dF}\omega_c(F) \tag{24}$$

for the existence of a critical force F_c. Therefore, we expect the same type of oscillatory limit cycle for collective catastrophe and rescue oscillations for a large class of catastrophe models which meet the two conditions stated in Sec. II B: (i) The catastrophe rate $\omega_c = \omega_c(v_+)$ is a function of the growth velocity only and (ii) the resulting force dependence fulfills condition (24), which gives rise to a catastrophe rate increasing exponentially with force above the characteristic force F_0. Whereas the Flyvbjerg and Janson catastrophe models and, more generally, all models with $\omega_c \propto v_+^{-\varepsilon}$ ($\varepsilon > 0$) fulfill condition (24), it is violated for the linear catastrophe model Eq. (5).

This explains that the mean-field result of an oscillatory limit cycle is robust with respect to variations of the catastrophe models: We expect qualitatively similar behavior for all catastrophe rates $\omega_c(F)$, which are exponentially increasing with force above a characteristic force F_0, for example, in the standard catastrophe models by Flyvbjerg *et al.* [4,5] or by Janson *et al.* [6]. This explains the robustness observed in the simulation results as shown in Figs. 4 and 5.

The condition (24) is violated for the linear catastrophe model Eq. (5). Accordingly, we do not expect to find an oscillatory limit cycle with collective catastrophe and rescue events. For this type of catastrophe model the nullclines are indeed no longer loop shaped, and the mean-field theory rather predicts a *stable* fixed point [see Fig. 8(a)]. Simulations confirm that collective catastrophe and rescue oscillations are absent for the linear catastrophe model, and we find a rather stationary position x of the obstacle and, thus, a stationary polymerization force [see Fig. 8(b)].

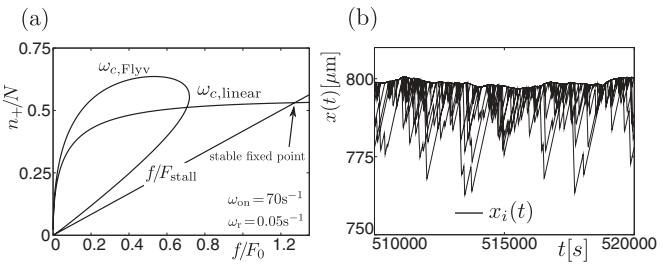

FIG. 8. (a) Nullclines of the mean-field equations for the linear model (5) with $\tilde{a} = 0.005\ \mathrm{s}^{-1}$ and $\tilde{b} = 8 \times 10^5\ \mathrm{m}^{-1}$. We use $\omega_{\mathrm{on}} = 70\ \mathrm{s}^{-1}$, $\omega_r = 0.05\ \mathrm{s}^{-1}$, and $k = 10^{-7}\ \mathrm{N/m}$ (soft barrier). The nullcline for $v_+ \equiv \langle n_+\rangle/N$ is not loop shaped. A stable fixed point exists at the intersection with the nullcline for f, which is the straight line $v_+ = f/F_{\mathrm{stall}}$. (b) Simulation trajectory of the position $x(t)$ of all MTs as a function of time t for $N = 10$.

VI. STOCHASTIC FLUCTUATIONS

The dynamical mean-field theory explains all simulation results qualitatively. In order to obtain quantitative agreement with stochastic simulations, we have to take into account that the maximal force F_{max} for a collective catastrophe is typically *smaller* than the critical mean-field force F_c [see Figs. 5(a) and 5(c)] because of additional stochastic fluctuations of n_+, which reduce the first passage time to a shrinking state $n_+ = 0$ (see Fig. 7).

Improved mean-field results including this effect [28] agree quantitatively with full stochastic simulations [see Figs. 5(a) and 5(c)]. We confirm the *linear* N dependence of the time-averaged force $F_{s,N}$ for small $N < 10$ and find a slightly stronger than linear increase for larger N. We also reproduce the approximately increase of $F_{s,N}$ with the on-rate ω_{on} [see Figs. 5(b) and 5(d)].

VII. CONCLUSION

In cooperative force generation by an ensemble of N MTs, the interplay between force sharing and MT dynamic instability gives rise to a complex dynamics, which can be described in terms of collective catastrophe and rescue events.

We developed a dynamical mean-field theory [see Eqs. (15) and (16)] which gives a quantitative description of the cooperative MT dynamics in terms of two parameters, the mean force $\langle F\rangle$ and the mean number of pushing MTs $\langle n_+\rangle$, in both the absence and presence of rescue events. Using this mean-field theory we identify the relevant control parameters, such as tubulin on-rate, rescue rate, and MT number, and their influence on force generation, and we investigate the robustness against variations of the catastrophe model. We validated the dynamical mean-field theory by stochastic simulations of the MT ensemble dynamics.

Our main findings are as follows. In the absence of rescue events, the maximal polymerization force before collective catastrophes grows linearly with N for small N or a stiff elastic barrier, in agreement with existing experimental data [11], whereas it crosses over to a logarithmic dependence for larger N or soft elastic barrier [see Eq. (10) and Fig. 3]. This crossover should be accessible in experiments by varying the stiffness of optical traps.

In the presence of rescue events and for a *soft* elastic barrier, the dynamics becomes strongly modified: Collective catastrophes and rescues lead to an oscillatory stable limit cycle dynamics far from a Hopf bifurcation. These oscillations should be observable *in vitro* in experiments such as in Ref. [11] if the MT lengths are sufficient to observe rescue events and if the stiffness of optical traps is reduced. Moreover, *in vivo* the behavior of polarized MT ensembles can be explored, as has been shown in Ref. [9], and our model predicts synchronized growth and shrinkage in oscillations if a polarized MT ensemble is growing against an elastic barrier such as the cell cortex.

In the presence of oscillations, we have quantified the maximal polymerization force $F_c = Nf_c$ in Eq. (20) and the time-averaged polymerization force $F_{s,N}$ in Eq. (23). Both forces are *linear* in N [see Figs. 5(a) and 5(d)], and the relevant force scale is the force scale F_0, above which the MT growth velocity decreases exponentially and the MT catastrophe rate increases exponentially. The linear N dependence of forces in the presence of rescue events is remarkable because we find an only logarithmic increase with N in the absence of rescue events for soft barriers (see Fig. 3). Nevertheless, even the maximal polymerization force is significantly smaller than the N-fold single-MT stall force. This shows that MTs are not optimized with respect to force generation because of their dynamic instability, even if they cooperate in an ensemble. On the other hand, our analysis also shows that force generation in MT ensembles is very sensitive to changes of system parameters related to the dynamic instability of MTs; in particular, it strongly increases with increasing tubulin on-rate (and, thus, decreasing catastrophe rate) or increasing MT rescue rate (see Fig. 5). The combination of both results suggests that a MT ensemble is not efficient to generate high forces but that the dynamic instability in connection with the ensemble dynamics allows us to efficiently regulate force generation through several system parameters. In the living cell, the on-rate can be changed by sequestering tubulin dimers and catastrophe and rescue rates are influenced, for example, by microtubule associated proteins [18,21,22].

Our results also have implications for possible mechanisms which determine the mean length of the MT cytoskeleton, as it has been studied experimentally in Ref. [9]. For a fixed stiffness k of the opposing elastic force, the average force generated by the MT ensemble corresponds to an average length of MTs. The linear increase of the average force with the number N of MTs suggests that the MT length and, eventually, the cell size should exhibit a similar linear increase with the number of MTs in a polarized MT cytoskeleton if the stiffness of the cell cortex remains unchanged.

In vivo, regulation mechanisms, which will involve the kinetics and spatial variation of concentrations of regulating proteins, will be relevant for cooperative MT dynamics and force generation. The present work provides a theory to describe the cooperative dynamics arising from force sharing and its dependence on various system parameters such as tubulin concentration and rescue rates. This is a prerequisite in order to explore spatial and temporal variations of these parameters in regulation mechanisms in future work.

ACKNOWLEDGMENTS

We acknowledge support by the Deutsche Forschungsgemeinschaft (KI 662/4-1).

[1] A. Desai and T. J. Mitchison, Annu. Rev. Cell Dev. Biol. **13**, 83 (1997).
[2] M. Dogterom and B. Yurke, Science **278**, 856 (1997).
[3] T. Mitchison and M. Kirschner, Nature **312**, 237 (1984).
[4] H. Flyvbjerg, T. E. Holy, and S. Leibler, Phys. Rev. Lett. **73**, 2372 (1994).
[5] H. Flyvbjerg, T. E. Holy, and S. Leibler, Phys. Rev. E **54**, 5538 (1996).
[6] M. Janson, M. de Dood, and M. Dogterom, J. Cell Biol. **161**, 1029 (2003).
[7] B. Zelinski, N. Müller, and J. Kierfeld, Phys. Rev. E **86**, 041918 (2012).
[8] J. McIntosh, E. Grishchuk, and R. West, Annu. Rev. Cell Dev. Biol. **18**, 193 (2002),
[9] R. Picone, X. Ren, K. D. Ivanovitch, J. D. W. Clarke, R. A. McKendry, and B. Baum, PLoS Biol. **8**, e1000542 (2010).
[10] F. E. Poulain and André Sobel, Mol. Cell. Neurosci. **43**, 15 (2010).
[11] L. Laan, J. Husson, E. L. Munteanu, J. W. J. Kerssemakers, and M. Dogterom, Proc. Natl. Acad. Sci. USA **105**, 8920 (2008).
[12] M. Dogterom and S. Leibler, Phys. Rev. Lett. **70**, 1347 (1993).
[13] X. Li, J. Kierfeld, and R. Lipowsky, Phys. Rev. Lett. **103**, 048102 (2009).
[14] X. Li, R. Lipowsky, and J. Kierfeld, Europhys. Lett. **89**, 38010 (2010).
[15] M. Abramowitz and A. I. Stegun, *Handbook of Mathematical Functions* (National Bureau of Standards, Washington, DC, 1965).
[16] M. K. Gardner, M. Zanic, C. Gell, V. Bormuth, and J. Howard, Cell **147**, 1092 (2011).
[17] M. E. Janson and M. Dogterom, Phys. Rev. Lett. **92**, 248101 (2004).
[18] D. N. Drechsel, A. A. Hyman, M. H. Cobb, and M. W. Kirschner, Mol. Biol. Cell **3**, 1141 (1992).
[19] R. F. Gildersleeve, A. R. Cross, K. E. Cullen, A. P. Fagen, and R. C. Williams, J. Biol. Chem. **267**, 7995 (1992).
[20] R. A. Walker, E. T. O'Brien, N. K. Pryer, M. F. Soboeiro, W. A. Voter, H. P. Erickson, and E. D. Salmon, J. Cell Biol. **107**, 1437 (1988).
[21] N. K. Pryer, R. A. Walker, V. P. Skeen, B. D. Bourns, M. F. Soboeiro, and E. D. Salmon, J. Cell Sci. **103**, 965 (1992).
[22] R. Dhamodharan and P. Wadsworth, J. Cell Sci. **108**, 1679 (1995).

[23] C. Nakao, T. J. Itoh, H. Hotani, and N. Mori, J. Biol. Chem. **279**, 23014 (2004).
[24] E. Shelden and P. Wadsworth, J. Cell Biol. **120**, 935 (1993).
[25] J. Krawczyk and J. Kierfeld, Europhys. Lett. **93**, 28006 (2011).
[26] M. F. Carlier, R. Melki, D. Pantaloni, T. L. Hill, and Y. Chen, Proc. Natl. Acad. Sci. USA **84**, 5257 (1987).
[27] A. Marx and E. Mandelkow, Eur. Biophys. J. **22**, 405 (1994).
[28] B. Zelinski and J. Kierfeld (to be published).